

CLINICAL AND IMAGING TOOLS IN THE EARLY DIAGNOSIS OF PROSTATE CANCER, A REVIEW*

P. De Visschere¹, W. Oosterlinck², G. De Meerleer³, G. Villeirs¹

Measurement of serum Prostate Specific Antigen (PSA) level is useful to detect early prostate cancer. PSA-screening may reduce the mortality rate from prostate cancer, but this is associated with a high rate of overdiagnosis and overtreatment. To improve the detection of clinically significant cancers, several auxiliary clinical and imaging tools can be used. The absolute PSA value can be complemented with parameters such as PSA velocity, PSA density and free/total PSA. Transrectal Ultrasound (TRUS) has only moderate accuracy in the detection of prostate carcinoma, but is very useful in the estimation of prostate volume and thus calculation of PSA-density. The role of Magnetic Resonance Imaging (MRI) in diagnosis and staging of prostate carcinoma is rapidly increasing. Morphologic T2-weighted MR images (T2-WI), preferably with an endorectal coil, depict the prostatic anatomy with high resolution and can detect tumoral areas within the peripheral zone of the prostate. Addition of MR spectroscopic imaging (MRSI), dynamic contrast enhanced MRI (DCE-MRI) and/or diffusion weighted imaging (DWI) further increase the diagnostic performance of MRI. The gold standard for diagnosis of prostate carcinoma is histological assessment obtained by transrectal ultrasound-guided systematic core needle biopsy. In the future, imaging-based targeted biopsies may improve the biopsy yield and decrease the number of biopsy cores. Computed Tomography (CT) and positron emission tomography (PET) have no value in early prostate cancer detection and the indications are limited to lymph node staging and detection of distant metastases.

Introduction

Prostate cancer is one of the most common tumors in Western countries, but not all detected cancers will become symptomatic during the patient's lifetime if left untreated (1-3). Treatment selection is based on prognostic factors such as serum Prostate Specific Antigen (PSA) level, histological grading (Gleason score), tumor size, clinical staging (TNM classification) and the patient's life expectancy and co-morbidity (1, 4, 5). On the basis of these variables, patients may be either allocated to active treatment (radical prostatectomy, radiotherapy, minimally invasive surgery) when the tumor is deemed clinically relevant, or to active surveillance when the impact of the prostate cancer on the patient's life expectancy and quality of life is deemed insignificant. Such allocations obviously require a highly accurate assessment of the above-mentioned prognostic factors. In this review article, the role of traditional clinical parameters (PSA, digital rectal examination, histological grading) will be discussed and the increasing role of imaging techniques to improve treatment stratification will be highlighted.

Clinical tools

PSA

Most prostate carcinomas are detected on the basis of elevated serum PSA, which is up to present the best available test for early detection of prostate carcinoma (3-6). Its exact cut-off level is age-dependent but remains controversial (7). Commonly > 3.0 ng/ml is used as the trigger for further examination (6). Apart from tumoral etiology, PSA levels may also be elevated due to benign prostatic hyperplasia (BPH), acute and chronic prostatitis and recent urologic procedures (1, 4, 7). To improve the differentiation between benign and malignant causes of PSA-elevation, additional parameters such as PSA velocity, PSA density and free/total PSA are frequently used (3, 5). PSA velocity is determined by the evolution of serum PSA over time. If the serum PSA increases > 0.75 ng/ml/year, there is a higher risk of clinically significant prostate cancer (3, 5). PSA density relates serum PSA level to the prostate volume, usually calculated with transrectal ultrasound (TRUS) or magnetic resonance imaging (MRI). A level below 0.15 ng/ml/cc is more suggestive of

benign prostatic hyperplasia (BPH) than of prostate carcinoma (5, 7). The percentage free/total PSA is used for further risk assessment in the PSA-range lower than 10 ng/ml; values above 25% are most frequently associated with BPH, whereas values under 10% are highly suggestive of malignancy, although chronic prostatitis may show similar low percentages (5, 7).

The impact of PSA screening on prostate cancer survival remains controversial (4, 6). Recent reports of large-scale randomized studies addressing the issues of population screening for prostate cancer (the Prostate, Lung, Colorectal, Ovarian cancer (PLCO) screening trial and the European Randomized Study of Screening for Prostate Cancer (ERSPC) trial) have demonstrated that PSA-based screening leads to a significant increase of prostate cancer detection and that numerous patients with prostate cancer are being identified at an earlier and potentially more treatable stage (8). As a result, the mortality rate from prostate cancer can be reduced by about 20%. Unfortunately, this can only be achieved at the cost of a high rate of overdiagnosis and overtreatment (9). To avoid overdiagnosis, the European Guidelines Committee advises no routine PSA testing in patients younger than 50 years, or in patients with a life expectancy of less than 10 years (5, 10). Recently another biomarker, Prostate Cancer Gene 3 (PCA3) has been developed. PCA3 is highly specific for prostate cancer and is not influenced by prostatitis. It has better diagnostic accuracy than PSA for prediction of

From: 1. Department of Radiology (Division of Genitourinary Radiology), 2. Department of Urology, 3. Department of Radiotherapy, Ghent University Hospital, Ghent, Belgium. Address for correspondence: P. De Visschere, Ghent University Hospital, De Pintelaan 185, 9000 Ghent, Belgium. E-mail: pmzgvvm@yahoo.com

* Paper presented at the Annual Symposium of RBRS in November 14, 2009.

prostate cancer but has not yet been compared to additional parameters such as PSA-density. Moreover, it is expensive and currently not remunerated in Belgium (6, 11-13).

Digital Rectal Examination

PSA-testing is in daily practice routinely supplemented with a digital rectal examination (DRE), to assess the prostatic shape, symmetry, firmness and nodularity, and to detect grossly enlarged prostate glands (14, 15). DRE primarily detects higher risk tumors and more advanced disease, but since the PSA-era the majority of detected prostate carcinomas is not palpable (1, 2, 4, 8). Although the overall diagnostic sensitivity is quite low and influenced by observer bias, it is nevertheless capable of finding about 15% of cancers that would otherwise go undetected by PSA screening alone (14).

Histology

The gold standard for diagnosis of prostate carcinoma is histological assessment (4). Histological specimens are obtained with ultrasound-guided transrectal core needle biopsy when PSA-results, DRE and/or imaging studies are not reassuring. Traditionally, systematic biopsies are performed with 6 to 12 cores, depending on the prostatic volume, but supplemental image-guided targeted biopsies may improve the detection rate of significant cancer and decrease the number of biopsy cores (16). An important histopathologic parameter is the Gleason score. It reflects the grade of differentiation of the prostate cancer and thus correlates with tumor aggressiveness (4, 16, 17). A score of 3 + 4 or lower corresponds to a less-aggressive tumor with lower risk of non-organ confined disease, while a score of 4 + 3 or higher corresponds to a more aggressive tumor with higher clinical significance and mortality risk.

Imaging tools

Transrectal Ultrasound (TRUS)

The prostate can be evaluated with a high-frequency intrarectal ultrasound transducer. The normal prostatic contour is usually clearly depicted and the isoechoic peripheral zone can be differentiated from the heterogeneous central gland (Fig. 1, 2). About 70% of prostate carcinomas are found within the peripheral zone (4, 10) and may be

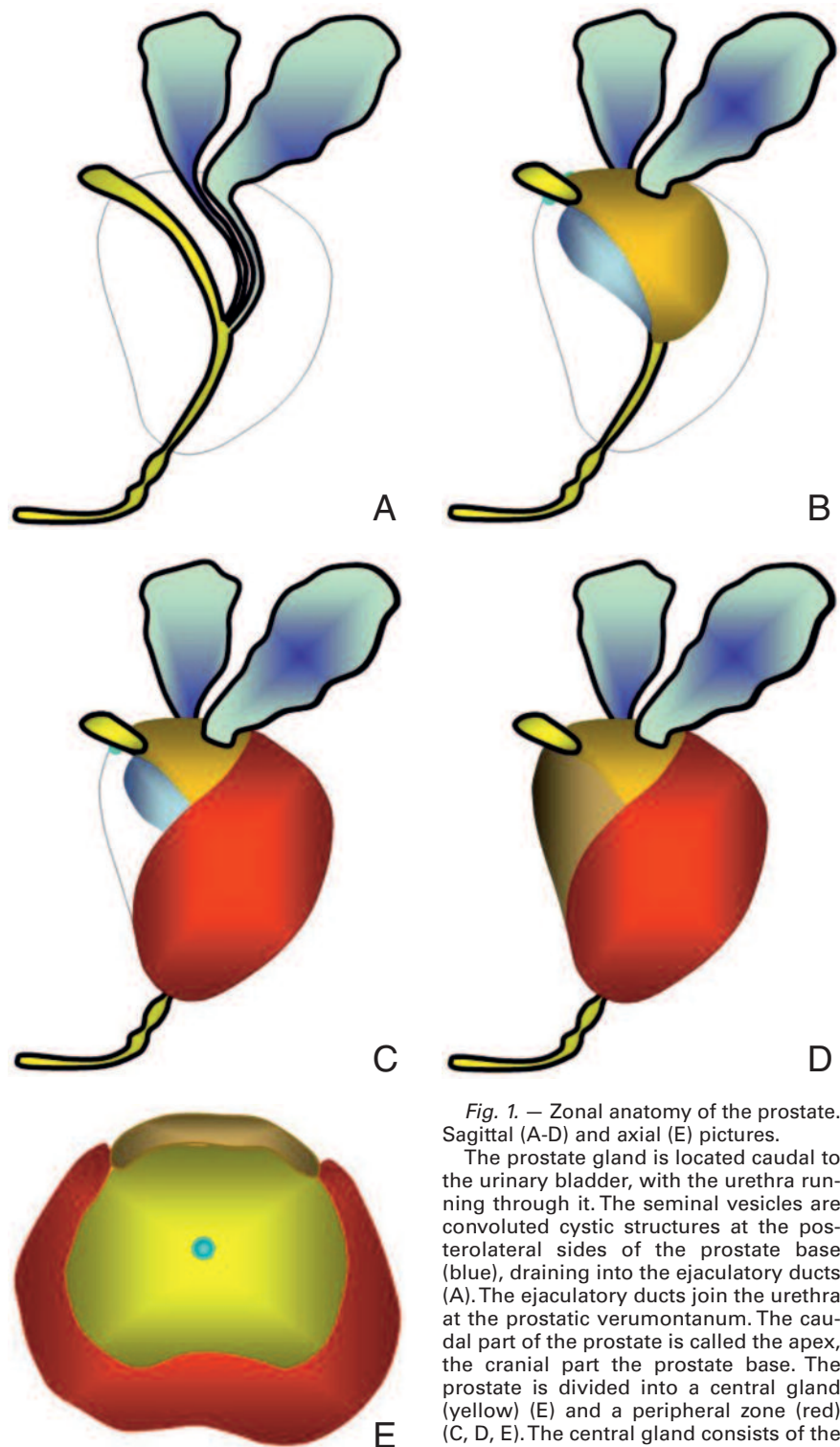


Fig. 1. — Zonal anatomy of the prostate. Sagittal (A-D) and axial (E) pictures.

The prostate gland is located caudal to the urinary bladder, with the urethra running through it. The seminal vesicles are convoluted cystic structures at the posterolateral sides of the prostate base (blue), draining into the ejaculatory ducts (A). The ejaculatory ducts join the urethra at the prostatic verumontanum. The caudal part of the prostate is called the apex, the cranial part the prostate base. The prostate is divided into a central gland (yellow) (E) and a peripheral zone (red) (C, D, E). The central gland consists of the periurethral glands along the proximal urethra, the paired pear-shaped transition

zones (gray) and the central zone, that envelops the ejaculatory ducts (orange) (B, E). In benign prostatic hyperplasia (BPH) the transition zone enlarges and compresses the central zone, which becomes a surgical pseudocapsule between the central gland and the peripheral zone. The peripheral zone is covered by a thin capsule, known as the true anatomic capsule. Anteriorly, the prostate is covered by the anterior fibromuscular stroma (brown) (D, E).

(Reprinted from Villeirs GM, Verstraete KL, De Neve WJ and De Meerleer GO, 2005, Magnetic Resonance Imaging Anatomy of the prostate and periprostatic area: a guide for radiotherapists, Radiotherapy and Oncology, 76, 99-106, copyright © 2005, with permission from Elsevier).

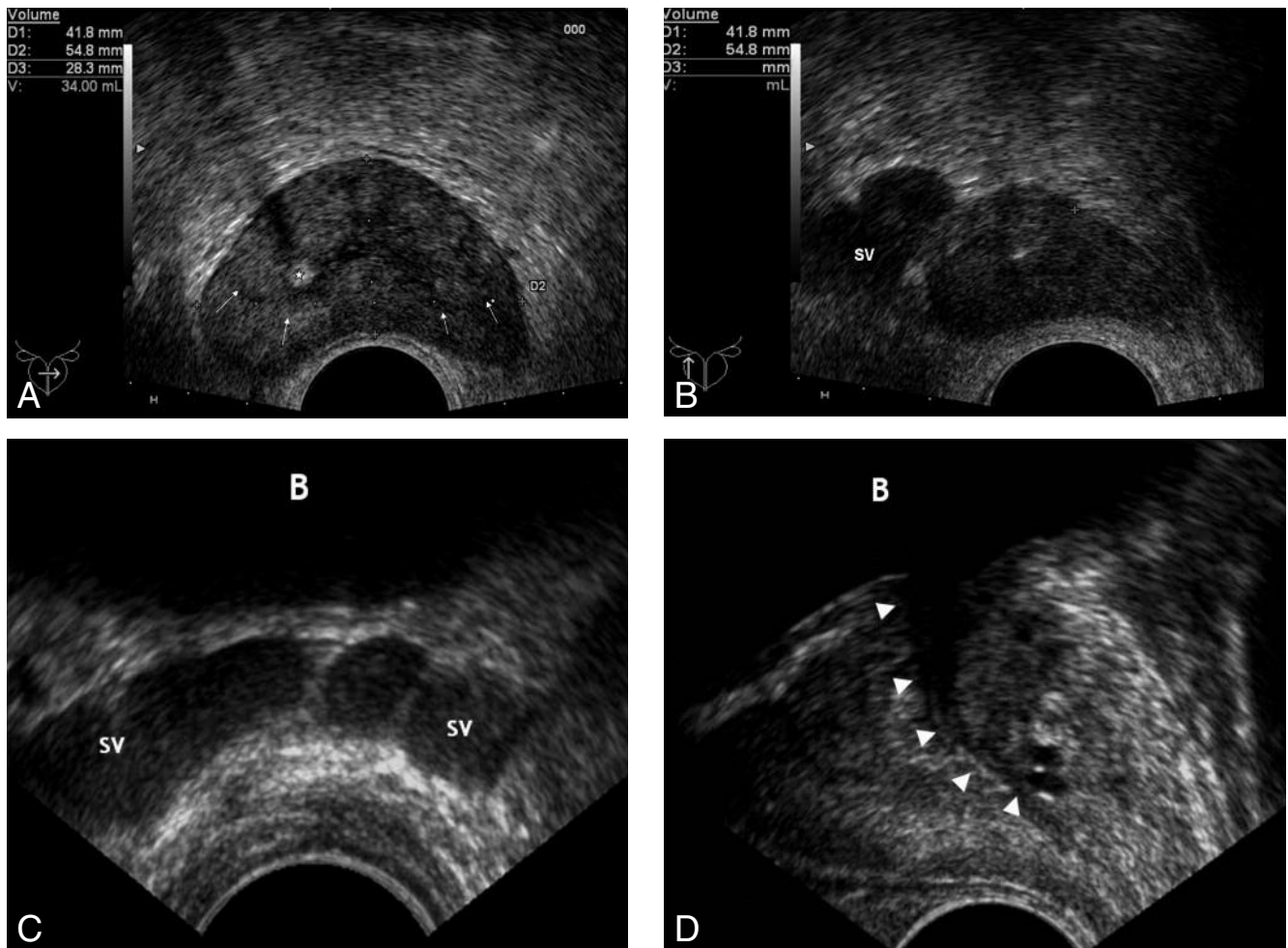


Fig. 2. — Transrectal ultrasound of the normal prostate in a 59-year old male, transverse (A, C) and sagittal (B, D) sections.

The prostate is located caudal to the bladder (B) (C, D). The prostatic contour is clearly depicted and can be used for volume estimation (A, B). The isoechoic peripheral zone may be differentiated from the hypo- or hyperechoic central gland (white arrows) (A). The seminal vesicles present as convoluted hypoechoic structures at both posterolateral sides of the prostate base (SV) (B, C). Sometimes central gland calcifications are visualised, with typical retroacoustic shadow (white star) (A). On sagittal sections the urethra running through the prostate is demonstrated (white arrowheads) (D).

visible as a predominantly hypoechoic area compared to normal peripheral zone tissue (Fig. 3). Tumors in the central gland are usually difficult to detect, because they blend with the heterogeneous central gland background tissue.

TRUS is widely available and is relatively cheap, but cannot be used in prostate cancer screening because it has only moderate accuracy for prostate cancer detection in the general population (1, 4, 18, 19). In patients with elevated PSA or an abnormal digital rectal examination (DRE), however, it can be used for initial morphologic assessment of the prostate and seminal vesicles, to measure the prostatic volume (for calculation of PSA density), or for biopsy guidance (1, 4, 18, 19). In an effort to improve the diagnostic accuracy of transrectal ultrasound, a number of ancillary techniques have

been proposed. Tumor neoangiogenesis can be detected with Doppler or Power-Doppler examinations, which are particularly helpful for the detection of isoechoic tumors that would normally be missed with gray-scale ultrasound (4, 10, 18). Intravenous injection of sonographic-contrast-media consisting of stabilized microbubbles, in conjunction with contrast harmonic techniques may further improve the sensitivity for increased blood perfusion (4, 18, 19). Tissue Harmonic Imaging results in improved spatial and contrast resolution (4, 10), and sono-elastography displays a color-coded qualification of tissue elasticity (4, 10, 18, 19), which helps to increase the positive biopsy yield of elastography-directed biopsies (20). Improved prostate cancer detection has also been reported with Tissue Type Imaging, a new technique which analyzes the

echo-signal spectrum before it is converted into an image (19, 21, 22).

Computed Tomography

Computed Tomography (CT) has little value in the detection of primary prostate cancer (1, 18). The margins of the lower prostate half are poorly defined on CT, and the intraprostatic anatomy is not sufficiently demonstrated (1), both on unenhanced or contrast-enhanced CT. CT can therefore not be used for prostate cancer detection and its indications are limited to lymph node staging or detection of distant metastases in patients with known prostate carcinoma (1, 18).

Magnetic Resonance Imaging (MRI)

The role of MRI in both the diagnosis and staging of prostate carcinoma has evolved tremendously in the past decade. In particular,

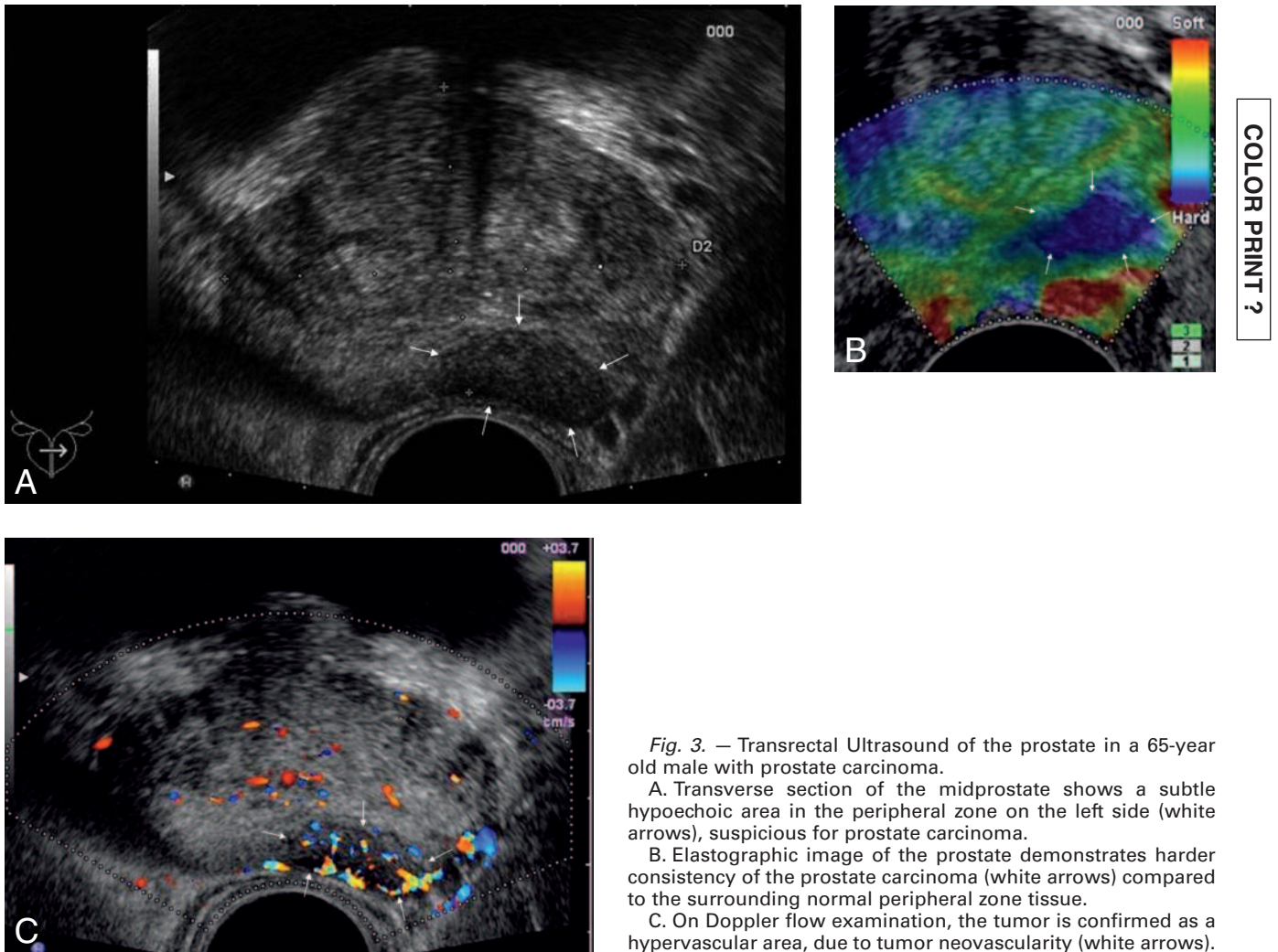


Fig. 3. — Transrectal Ultrasound of the prostate in a 65-year old male with prostate carcinoma.

A. Transverse section of the midprostate shows a subtle hypoechoic area in the peripheral zone on the left side (white arrows), suspicious for prostate carcinoma.

B. Elastographic image of the prostate demonstrates harder consistency of the prostate carcinoma (white arrows) compared to the surrounding normal peripheral zone tissue.

C. On Doppler flow examination, the tumor is confirmed as a hypervascular area, due to tumor neovascularity (white arrows).

the introduction of endorectal-coil imaging and the emergence of functional techniques such as MR spectroscopy (MRSI), dynamic contrast-enhanced MRI (DCE-MRI) and diffusion weighted imaging (DWI) has boosted the diagnostic accuracy of MRI and its potential to refine the therapeutic decision making process (1, 22). Standard morphologic imaging sequences should include 4 mm transverse, sagittal and coronal fast-T2 weighted images (Fig. 4) for tumor detection, localisation and staging (1, 4), supplemented with a 4 mm transverse breath-hold T1-weighted sequence for detection of post-biopsy intraglandular hemorrhage (Fig. 5) (1, 2, 4, 23). On 1.5T equipment, the use of an endorectal coil in conjunction with a pelvic phased-array coil is highly recommended (1, 2). It significantly increases the signal-to-noise ratio for prostate imaging and markedly improves spatial and contrast resolution. The balloon-covered endorectal coil is inflated with 60cc

of air or filled with 40cc of perfluorocarbon (PFC) to increase the magnetic field homogeneity by eliminating the air-tissue interface and reducing susceptibility artifacts (1, 2, 17, 22). Before the examination Scopolamine (Buscopan®) IV is administered to reduce peristaltic motion of the rectum and adjacent bowel segments (17).

T2-weighted sequences exquisitely depict the prostatic zonal anatomy and the presence and extent of low signal-intensity prostate carcinoma surrounded by high signal-intensity normal peripheral zone tissue (Fig. 6) (24). Because about 70% of all prostate cancers occur within the peripheral zone, many of them can readily be detected on morphologic T2-weighted images. Nevertheless, a low signal intensity area is not specific for prostate cancer, since benign conditions such as prostatitis, hemorrhage, hyperplastic nodules or post-treatment (hormonal or irradiation) changes may equally show low signal intensity (1, 2, 24,

25). Furthermore, morphologic T2-WI is less accurate for evaluating central gland cancers, unless they show an irregular area of uniform low signal-intensity (16, 26). Overall, diagnostic accuracies of about 70% have been reported for morphologic T2-WI in the detection of prostate cancer (24, 27, 28).

MR spectroscopy (MRSI) provides information about the relative concentrations of cellular metabolites in the prostate. A three-dimensional data set with spectra from small voxels of 0.5 cc or less is acquired throughout the prostate. MRSI sequences suppress signal contributions from water and fat and measure the relative concentrations of citrate, choline, creatine and polyamines, which resonate at distinct frequencies in the spectrum (1, 24, 29). Citrate is synthesized, stored and secreted by glandular tissue in the prostate and is abundantly available in the normal peripheral zone and in glandular benign prostatic hyperplasia (1) (Fig. 7). In prostate

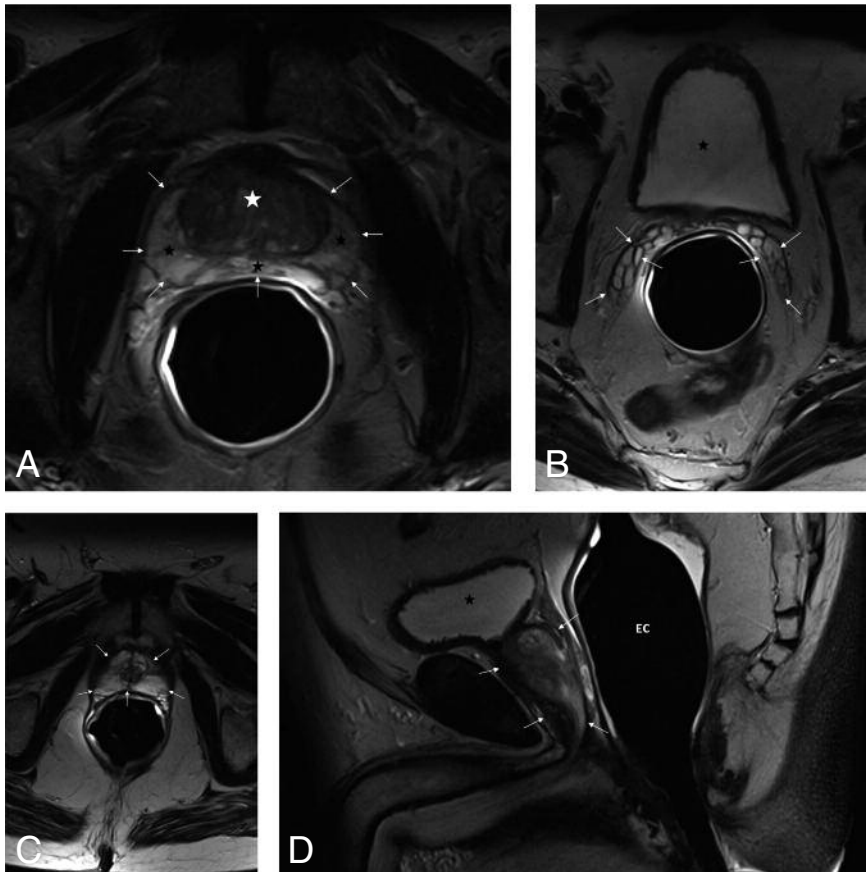


Fig. 4. — T2-weighted endorectal coil MR images of the normal prostate in a 63-year old male.

A. Transverse section at midprostatic level. The normal zonal anatomy is depicted with high resolution. The central gland shows a heterogeneous low signal intensity (white star), whereas the peripheral zone shows diffuse high signal intensity (black stars), surrounded by a thin rim of low signal intensity, which represents the anatomic or true capsule (white arrows).

B. Transverse section through the seminal vesicles. These are demonstrated as convoluted high-signal intensity lobules (white arrows) at both superolateral sides of the prostate.

C. Transverse section at level of the prostatic apex. The peripheral zone is demonstrated as high signal intensity tissue (white arrows) surrounding the hypointense external sphincter and urethra.

D. Sagittal section showing the prostate (white arrows), caudal to the urinary bladder (black star), and anterior to the rectum with the endorectal coil.

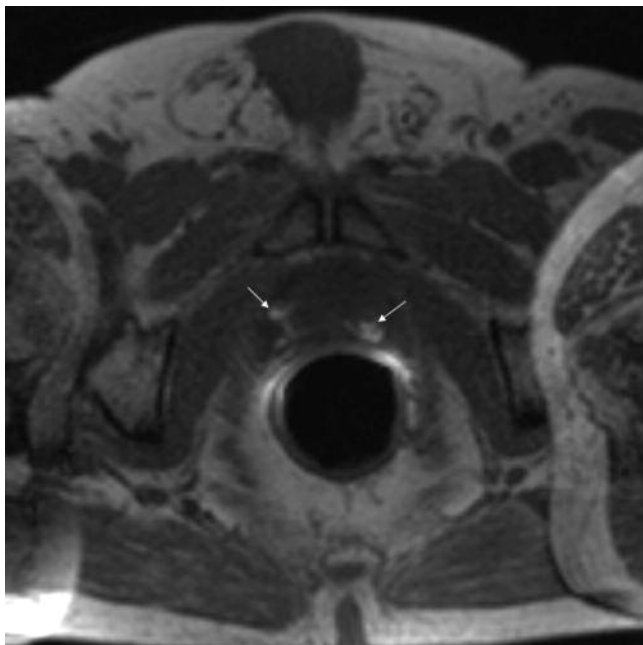


Fig. 5. — Transverse T1-weighted MR image of the prostate in a 75-year-old male 4 weeks after transrectal ultrasound-guided biopsy.

Post-biopsy artefacts are demonstrated as high signal intensity foci in the prostate on T1-weighted images (white arrows), as blood demonstrates high signal on these sequences.

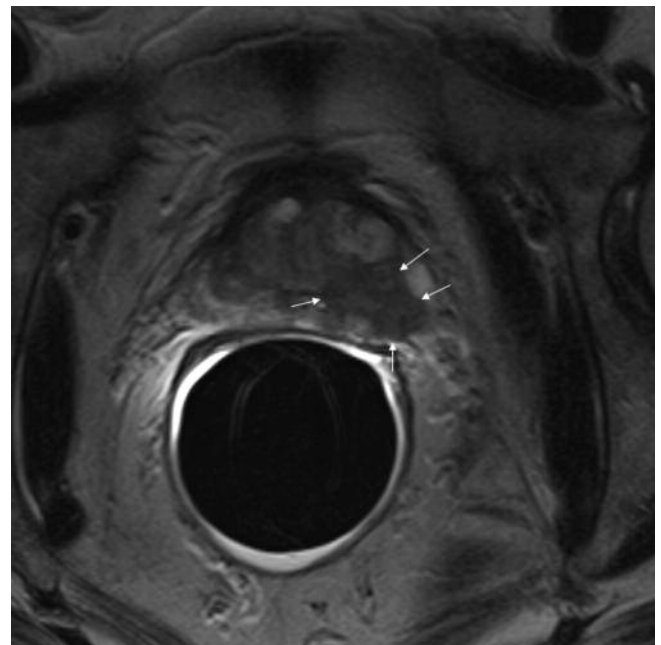


Fig. 6. — Transverse T2-weighted MR image in a 77-year-old male with prostate cancer.

The tumor is demonstrated as a circumscribed low signal-intensity lesion in the peripheral zone of the prostate (white arrows).

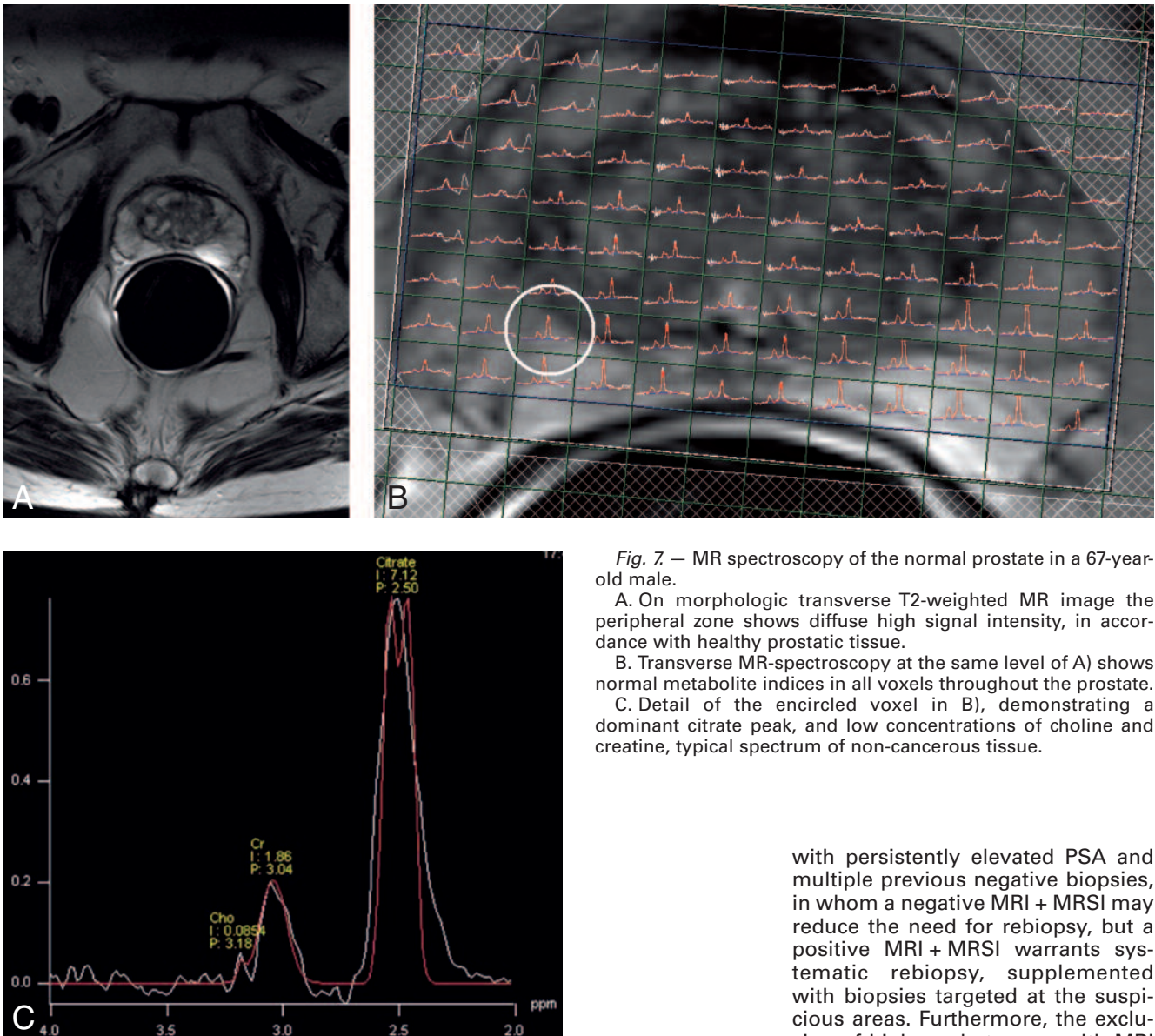


Fig. 7. — MR spectroscopy of the normal prostate in a 67-year-old male.

A. On morphologic transverse T2-weighted MR image the peripheral zone shows diffuse high signal intensity, in accordance with healthy prostatic tissue.

B. Transverse MR-spectroscopy at the same level of A) shows normal metabolite indices in all voxels throughout the prostate.

C. Detail of the encircled voxel in B), demonstrating a dominant citrate peak, and low concentrations of choline and creatine, typical spectrum of non-cancerous tissue.

carcinoma, however, the citrate level is significantly reduced, in part because of oxidation of citrate (29). Choline is an important constituent in the cell membrane metabolism and its concentration increases in highly cellular areas, such as tumor lesions (29). The contributions of polyamines and creatine are less important. Polyamines are reduced or absent in prostate cancer (30), but on 1.5T clinical MRI scanners, they cannot be entirely resolved from choline and creatine peaks (1). The creatine peak is not substantially different in cancer than in normal peripheral zone tissue and is included in the analysis only to ease the quantification of choline compounds (1, 31).

The complimentary changes of these metabolites are used to predict the presence or absence of prostate

cancer by means of the choline-plus-creatine-to-citrate (CC/C) ratio, in which higher ratios are increasingly more suggestive of prostate cancer. Diagnostic accuracies up to 70-90% for MRI combined with MRSI have been reported, yielding a 20% improvement compared to morphologic T2-WI alone (Fig. 8) (24, 28, 29, 32). Interestingly, the CC/C ratio has also been shown to correlate with the Gleason score, therefore MRSI has the potential to non-invasively assess tumor aggressiveness (1, 2, 29). In our own investigation in 356 men with elevated PSA (33) the combination of MRI and MRSI was able to predict the presence or absence of high grade (Gleason 4 + 3 or higher) prostate carcinoma with a sensitivity of 92,7%, and a negative predictive value of 98,5%. This is of particular importance in patients

with persistently elevated PSA and multiple previous negative biopsies, in whom a negative MRI + MRSI may reduce the need for rebiopsy, but a positive MRI + MRSI warrants systematic rebiopsy, supplemented with biopsies targeted at the suspicious areas. Furthermore, the exclusion of high grade tumors with MRI + MRSI may support the choice for active surveillance in a prostate cancer patient in whom active therapy is deemed inappropriate.

In dynamic contrast enhanced MRI (DCE-MRI) the prostate is evaluated on serial (every 2-5 sec) 3D GE T1-WI after intravenous bolus injection (0.1 mmol/kg) of a low-molecular weight contrast agent (Gadolinium chelate) (1, 17). Alternatively, T2*-sequences have been designed that are sensitive to tissue perfusion and blood volume, but up to present there are only limited data on these methods (2, 24). Prostate carcinoma is associated with de novo angiogenesis, increased microvessel density and increased vascular permeability. Most prostate carcinomas show earlier and higher peak enhancement with initial steep slope of the signal intensity – time curve, as well as early washout (1,

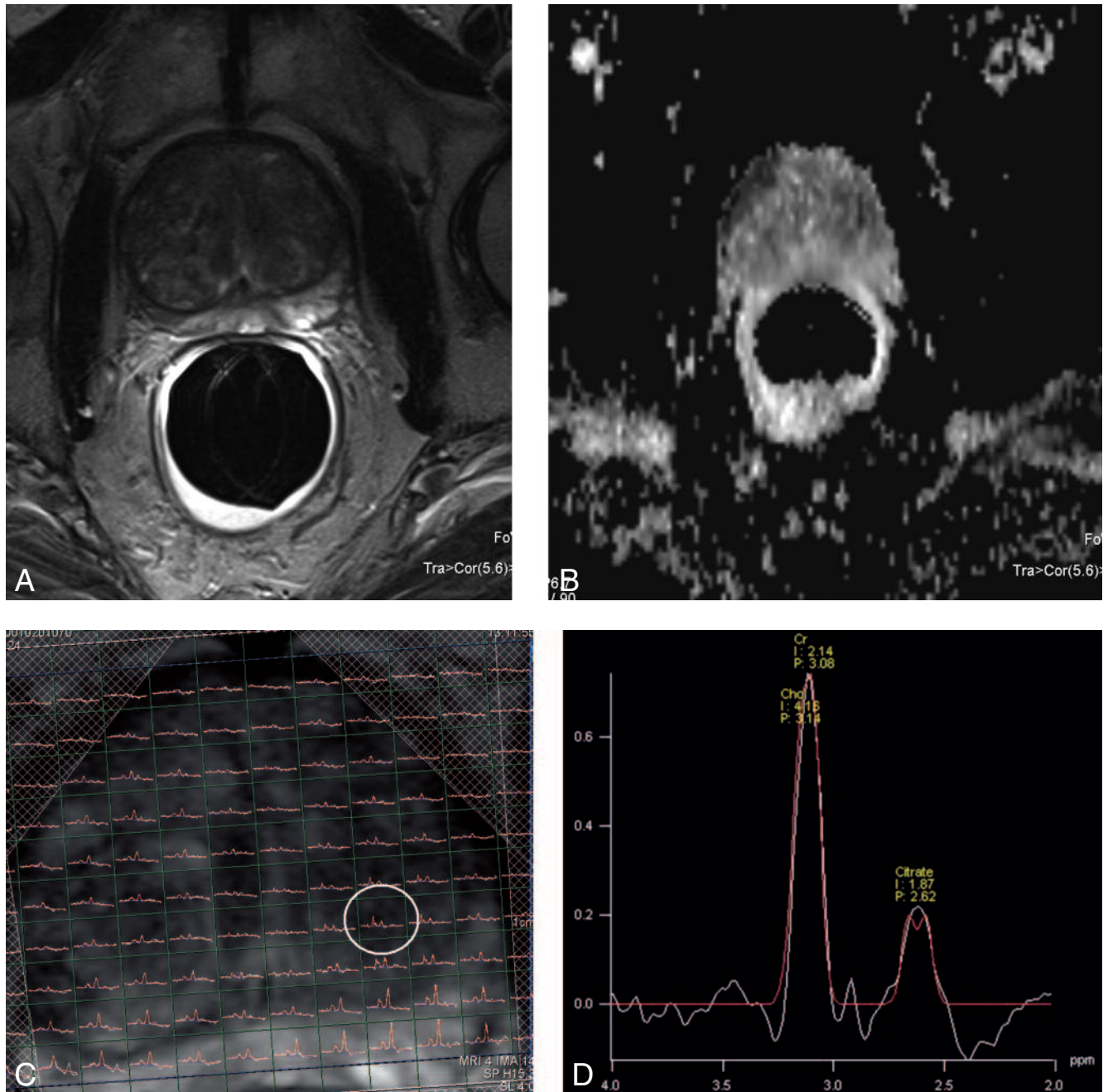


Fig. 8. — 78-year-old male with prostate carcinoma in the central gland on the left side.

A. On T2-weighted MR images there is normal high signal intensity in the peripheral zone. The central gland shows heterogeneous low signal intensity.

B. Diffusion weighted MR image at the same level as a) demonstrates no restricted diffusion.

C. MR-spectroscopy at the same level as A) and B) reveals reduced citrate levels and high choline levels in several voxels in the central gland on the left side, suspicious for prostate carcinoma.

D. Detail of the encircled voxel in C), demonstrating a dominant choline peak and decreased concentration of citrate: typical spectrum of prostate cancer.

17). Several quantitative postprocessing parameters have been developed, such as K^{trans} (= transfer constant or the permeability surface area, relating the fraction of contrast agent transferred from blood to the interstitial space), v_e (= extravascular extracellular space (EES) or interstitial space) and k_{ep} (= rate constant,

representing the efflux from the EES to blood plasma) (1, 17, 23, 27). Most prostate carcinomas show an increased vascular permeability K^{trans} and higher k_{ep} (17). However, there still appears to be some overlap in the enhancement patterns between tumors and benign conditions such as prostatitis, postbiopsy hemor-

rhage and benign prostatic hyperplasia (27). Accuracies of 70 to 90% have been reported for dynamic contrast enhanced MRI in primary diagnosis of prostate carcinoma, again yielding a 20% improvement compared to morphologic T2-WI alone (17, 27).

Diffusion weighted imaging (DWI)

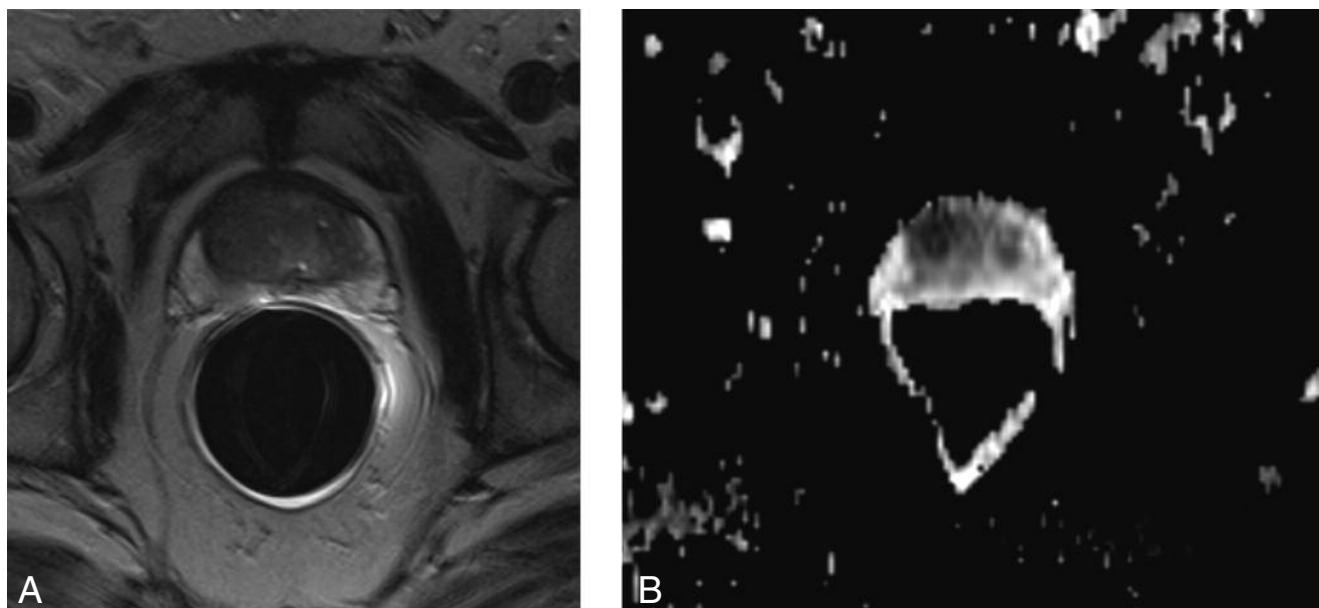


Fig. 9. — 70-year-old patient with prostate cancer in the central gland.

A. Morphologic T2-weighted MR image through the midprostate shows normal high signal intensity in the peripheral zone. The central gland shows diffuse low signal intensity.

B. Apparent diffusion coefficient map, corresponding to A) demonstrates restricted diffusion on the right side in the central gland. Targeted biopsy under transrectal ultrasound-guidance, confirmed prostate cancer in this area.

provides information about the amount of random 'Brownian' movements of water molecules. 4 mm single-shot fat-suppressed echo-planar images (EPI) are acquired at various gradients of diffusion (b -values = 0, 250, 500, 750 and 1000 s/mm²), with calculation of an apparent diffusion coefficient (ADC) (23, 24). The degree of diffusion of protons is dependent on tissue density, cell organisation and binding to macromolecules. Protons are very mobile in normal acinous water-rich glandular tissue, but restricted in their movement in densely packed water-poor tissue such as tumor areas, which contain many hydrophobic cell membranes (24). As a consequence, prostate cancer in both the peripheral zone and transition zone displays significantly lower ADC values compared to benign prostatic tissue (2, 23, 24, 34) (Fig. 9). Increased tumour detection with DWI and a correlation between Gleason score and ADC values have been reported by several authors but the overall diagnostic efficacy still remains unclear (2, 23-25, 35-38).

Positron Emission Tomography (PET)

FDG-PET has a disappointingly low sensitivity for prostate cancer detection, with no difference in tracer uptake between benign prostatic hyperplasia and prostate carcinoma (1). New tracers such as

¹¹C Choline and ¹⁸F Fluorocholine are promising (18) as they show lower streak artifacts arising from the tracer-filled bladder and their very high sensitivity. Due to their low specificity they are not recommended for detection of primary prostate carcinoma (39-41), but are gaining acceptance in lymph node staging and in treatment follow up in patients with biochemical evidence of recurrence (1).

Conclusion

Most prostate carcinomas are detected on the basis of elevated serum PSA levels but the gold standard for diagnosis of prostate carcinoma is histological assessment. Transrectal ultrasonography has a low diagnostic yield in detection of prostate carcinoma and is therefore not recommended for screening, but is useful for calculation of prostatic volume and for biopsy guidance. CT and PET are not indicated in the detection of primary prostate cancer and are reserved for lymph node staging and detection of distant metastases. MR imaging, particularly the combination of endorectal coil T2-weighted morphologic imaging with functional MRI techniques such as MR spectroscopy, Diffusion Weighted MRI and Dynamic Contrast Enhanced MRI will undoubtedly play an increasing role in the early detection and characterization of prostate

cancer, especially of high grade tumors. MRI is not a first-line approach for the diagnosis of prostate cancer, but it may improve the diagnostic yield of targeted biopsy, especially in patients with persistently increased PSA levels but negative previous biopsies. Exclusion of high grade cancer is of particular interest in patients with prostate cancer who choose for active surveillance.

References

1. Fuchsjager M., Shukla-Dave A., Akin O., Barentsz J., Hricak H.: Prostate cancer imaging. *Acta Radiol*, 2008, 49: 107-120.
2. Mazaheri Y., Shukla-Dave A., Muellner A., Hricak H.: MR imaging of the prostate in clinical practice. *Magma*, 2008, 21: 379-392.
3. Catalona W.J., Loeb S.: The PSA era is not over for prostate cancer. *Eur Urol*, 2005, 48: 541-545.
4. Candefjord S., Ramser K., Lindahl O.A.: Technologies for localization and diagnosis of prostate cancer. *J Med Eng Technol*, 2009, 33: 585-603.
5. Verbaeys C., Oosterlinck W.: Prostaatspecifiek antigeen (PSA): indicatie, interpretatie en therapeutisch gevolg. *Tijdschrift voor Geneeskunde*, 2008, 64: 609-613.
6. Schroder F.H., Roobol M.J.: Defining the optimal prostate-specific antigen threshold for the diagnosis of prostate cancer. *Curr Opin Urol*, 2009, 19: 227-231.

7. Catalona W.J., Southwick P.C., Slawin K.M., et al.: Comparison of percent free PSA, PSA density, and age-specific PSA cutoffs for prostate cancer detection and staging. *Urology*, 2000, 56: 255-260.
8. Shteynshlyuger A., Andriole G.L.: Prostate cancer: to screen or not to screen? *Urol Clin North Am*, 37: 1-9, Table of Contents.
9. Schroder F.H., Hugosson J., Roobol M.J., et al.: Screening and prostate-cancer mortality in a randomized European study. *N Engl J Med*, 2009, 360: 1320-1328.
10. Pallwein L., Mitterberger M., Pelzer A., et al.: Ultrasound of prostate cancer: recent advances. *Eur Radiol*, 2008, 18: 707-715.
11. Lin D.W.: Beyond P.S.A.: utility of novel tumor markers in the setting of elevated PSA. *Urol Oncol*, 2009, 27: 315-321.
12. Schilling D., de Reijke T., Tombal B., de la Taille A., Hennenlotter J., Stenzl A.: The Prostate Cancer Gene 3 assay: indications for use in clinical practice. *BJU Int*, 2009, 105: 452-455.
13. Kirby R.S., Fitzpatrick J.M., Irani J.: Prostate cancer diagnosis in the new millennium: strengths and weaknesses of prostate-specific antigen and the discovery and clinical evaluation of prostate cancer gene 3 (PCA3). *BJU Int*, 2009, 103: 441-445.
14. Kijviki K.: Digital rectal examination, serum prostatic specific antigen or transrectal ultrasonography: the best tool to guide the treatment of men with benign prostatic hyperplasia. *Curr Opin Urol*, 2009, 19: 44-48.
15. Bosch J.L., Bohnen A.M., Groeneveld F.P.: Validity of digital rectal examination and serum prostate specific antigen in the estimation of prostate volume in community-based men aged 50 to 78 years: the Krimpen Study. *Eur Urol*, 2004, 46: 753-759.
16. Lawrentschuk N., Fleshner N.: The role of magnetic resonance imaging in targeting prostate cancer in patients with previous negative biopsies and elevated prostate-specific antigen levels. *BJU Int*, 2009, 103: 730-733.
17. McMahon C.J., Bloch B.N., Lenkinski R.E., Rofsky N.M.: Dynamic contrast-enhanced MR imaging in the evaluation of patients with prostate cancer. *Magn Reson Imaging Clin N Am*, 2009, 17: 363-383.
18. Afnan J., Tempany C.M.: Update on prostate imaging. *Urol Clin North Am*, 37: 23-25, Table of Contents.
19. Gravas S., Mamoulakis C., Rioja J., et al.: Advances in ultrasound technology in oncologic urology. *Urol Clin North Am*, 2009, 36: 133-145, vii.
20. Pallwein L., Mitterberger M., Struve P., et al.: Comparison of sonoelastography guided biopsy with systematic biopsy: impact on prostate cancer detection. *Eur Radiol*, 2007, 17: 2278-2285.
21. Feleppa E.J., Porter C.R., Ketterling J., et al.: Recent developments in tissue-type imaging (TTI) for planning and monitoring treatment of prostate cancer. *Ultrason Imaging*, 2004, 26: 163-172.
22. Kim C.K., Park B.K.: Update of prostate magnetic resonance imaging at 3 T. *J Comput Assist Tomogr*, 2008, 32: 163-172.
23. Somford D.M., Futterer J.J., Hambroek T., Barentsz J.O.: Diffusion and perfusion MR imaging of the prostate. *Magn Reson Imaging Clin N Am*, 2008, 16: 685-695, ix.
24. Seitz M., Shukla-Dave A., Bjartell A., et al.: Functional magnetic resonance imaging in prostate cancer. *Eur Urol*, 2009, 55: 801-814.
25. Van As N., Charles-Edwards E., Jackson A., et al.: Correlation of diffusion-weighted MRI with whole mount radical prostatectomy specimens. *Br J Radiol*, 2008, 81: 456-462.
26. Li H., Sugimura K., Kaji Y., et al.: Conventional MRI capabilities in the diagnosis of prostate cancer in the transition zone. *AJR Am J Roentgenol*, 2006, 186: 729-742.
27. Ocak I., Bernardo M., Metzger G., et al.: Dynamic contrast-enhanced MRI of prostate cancer at 3 T: a study of pharmacokinetic parameters. *AJR Am J Roentgenol*, 2007, 189: 849.
28. Futterer J.J., Heijmink S.W., Scheenen T.W., et al.: Prostate cancer localization with dynamic contrast-enhanced MR imaging and proton MR spectroscopic imaging. *Radiology*, 2006, 241: 449-458.
29. Kurhanewicz J., Vigneron D.B.: Advances in MR spectroscopy of the prostate. *Magn Reson Imaging Clin N Am*, 2008, 16: 697-710, ix-x.
30. Shukla-Dave A., Hricak H., Moskowitz C., et al.: Detection of prostate cancer with MR spectroscopic imaging: an expanded paradigm incorporating polyamines. *Radiology*, 2007, 245: 499-506.
31. Kurhanewicz J., Vigneron D., Hricak H., Narayan P., Carroll P., SJ. N. Three-dimensional H-1 MR spectroscopic imaging of the in situ human prostate with high (0.24-0.7-cm³) spatial resolution. *Radiology*, 1996,, 198: 795-805.
32. Zakian K.L., Sircar K., Hricak H., et al.: Correlation of proton MR spectroscopic imaging with Gleason score based on step-section pathologic analysis after radical prostatectomy. *Radiology*, 2005, 234: 804-814.
33. Villeirs G.M., De Meerleer G.O., De Visschere P.J., Fonteyne V.H., Verbaeys A.C., Oosterlinck W.: Combined magnetic resonance imaging and spectroscopy in the assessment of high grade prostate carcinoma in patients with elevated PSA: A single-institution experience of 356 patients. *Eur J Radiol*, 2009.
34. Sato C., Naganawa S., Nakamura T., et al.: Differentiation of noncancerous tissue and cancer lesions by apparent diffusion coefficient values in transition and peripheral zones of the prostate. *J Magn Reson Imaging*, 2005, 21: 258-262.
35. Yoshimitsu K., Kiyoshima K., Irie H., et al.: Usefulness of apparent diffusion coefficient map in diagnosing prostate carcinoma: correlation with stepwise histopathology. *J Magn Reson Imaging*, 2008, 27: 132-139.
36. Chen M., Dang HD., Wang JY., et al.: Prostate cancer detection: comparison of T2-weighted imaging, diffusion-weighted imaging, proton magnetic resonance spectroscopic imaging, and the three techniques combined. *Acta Radiol*, 2008, 49: 602-610.
37. desouza N.M., Reinsberg S.A., Scurr E.D., Brewster J.M., Payne G.S.: Magnetic resonance imaging in prostate cancer: the value of apparent diffusion coefficients for identifying malignant nodules. *Br J Radiol*, 2007, 80: 90-95.
38. Haider M.A., Chung P., Sweet J., et al.: Dynamic contrast-enhanced magnetic resonance imaging for localization of recurrent prostate cancer after external beam radiotherapy. *Int J Radiat Oncol Biol Phys*, 2008, 70: 425-430.
39. Emonds K.M., Swinnen J.V., Mortelmans L., Mottaghy F.M.: Molecular imaging of prostate cancer. *Methods*, 2009, 48:, 193-199.
40. Grenier N., Quesson B., de Senneville B.D., Trillaud H., Couillaud F., Moonen C.: Molecular MR imaging and MR-guided ultrasound therapies in cancer. *Jbr-Btr*, 2009, 92: 8-12.
41. Bouchelouche K., Oehr P.: Recent developments in urologic oncology: positron emission tomography molecular imaging. *Curr Opin Oncol*, 2008, 20: 321-326.